J Mater Sci (2012) 47:4075–4086
DOI 10.1007/s10853-012-6261-1

Effect of welding parameters on microstructure and mechanical properties of friction stir welded 2219Al-T6 joints

Z. Zhang · B. L. Xiao · Z. Y. Ma

Received: 28 October 2011 / Accepted: 7 January 2012 / Published online: 25 January 2012

Abstract The effect of friction stir welding (FSW) parameters on the microstructure and mechanical properties of 5.6 mm thick 2219Al-T6 joints was investigated in detail. While the sound FSW joints could be obtained under lower rotation rates of 400–800 rpm and welding speeds of 100–800 mm/min; higher rotation rates of 1200–1600 rpm easily led to the tunnel and void defects. The FSW thermal cycle resulted in low hardness zones (LHZs) on both retreating side (RS) and advancing side (AS). The LHZs may be located at the interface between the nugget zone (NZ) and the thermo-mechanically affected zone (TMAZ), at the TMAZ, or at the heat affected zone under the varied welding parameters. The tensile strength of FSW 2219Al-T6 joints increased when increasing the welding speed from 100 to 800 mm/min, and was weakly dependent on the rotation rates from 400 to 1200 rpm. The FSW 2219Al-T6 joints fractured along the LHZ on the RS.

Introduction

2xxx series aluminum alloys are widely used in aerospace and automobile industries due to their high strength and good damage tolerance [1, 2]. The 2219Al alloy is one of the most widely used aluminum alloys due to its excellent weldability by conventional fusion welding technologies [3]. However, the gap between the strength values of the fusion joints and the base material (BM) is very large (≥40%). Moreover, the poor solidification microstructure and porosity are unavoidable in the fusion welds of the 2219Al alloy due to melting and resolidification under the high heat input [4], damaging the mechanical properties of the fusion welds.

Friction stir welding (FSW) is a solid-state joining technique, invented by The Welding Institute (TWI) of UK in 1991 [5]. Because of the low heat input and the absence of a melting and solidification process, FSW could create high quality welds without pore and cracking, and was therefore very suitable for joining the aerospace aluminum alloys. It is currently being applied to the aerospace, automotive and shipbuilding industries and is attracting increasing research interest [6–8]. Thus, FSW is becoming a new alternative welding technology for the 2219Al alloy.

Compared with conventional fusion welding, different zones are produced by friction heat and plastic deformation during FSW. Under the drive of the welding tool (shoulder and pin), several different zones were produced on the transverse cross section of the FSW joint; i.e., nugget zone (NZ), thermo-mechanically affected zone (TMAZ), and heat affected zone (HAZ) on both retreating side (RS) and advancing side (AS), respectively. Several parameters, such as rotation rate (R), welding speed (V), geometry of the tool and the pin, tool tilt angle and its penetration into the blanks (plunge depth), affect the FSW process. Among these parameters, rotation rate and welding speed strongly influence the thermal cycle and are the two most important welding parameters.

For FSW precipitation-hardened (2xxx, 6xxx, and 7xxx) aluminum alloys, it was generally reported that the HAZ is the low hardness zone (LHZ) due to significant dissolution/coarsening of the precipitates during the FSW thermal cycle [9–15]. A number of studies showed that the FSW

Z. Zhang · B. L. Xiao · Z. Y. Ma (✉)
Shenyang National Laboratory for Materials Science, Institute of Metal Research, Chinese Academy of Sciences, 72 Wenhua Road, Shenyang 110016, China
e-mail: zyma@imr.ac.cn

joints of 6061Al-T651 [9, 10], 7050Al-T651 [11], 7050Al-T7451 [12], 7075Al-T651 [11, 13], and 2014Al-T651 [14] fractured along the LHZ during the tensile test. In this case, the properties of the HAZ dominated the mechanical properties of the FSW joints. It was reported that the tensile strength of the FSW aluminum alloy joints increased when increasing the welding speed, and was independent of the rotation rate [10, 14–18]. This has been reasonably explained by the microstructural evolution in the HAZ [10, 15] and further verified by thermal modeling [19, 20]. However, it was also found that FSW 2024Al-T351 joints would fracture along the segregation bands (a kind of linear structure with segregated second phase) at the NZ/TMAZ interface or at the NZ under some FSW parameters [15, 21]. These findings indicate that the effect of the FSW parameters on the mechanical properties and fracture behavior is complicated.

In the past few years, the 2219Al alloy has been subjected to extensive FSW investigations [22–26]. Chen et al. [22] and Liu et al. [23] reported that, at a constant rotation rate of 800 rpm, FSW 2219Al-T6 joints fractured at the HAZ and their tensile strength increased when increasing the welding speeds from 60 to 200 mm/min, but the void defects were produced at a high welding speed of 300 mm/min. Xu et al. [24] reported that the tensile strength of the FSW 2219Al-T6 joints increased from 295 to 329 MPa when increasing the rotation rate from 800 to 1100 rpm at a constant welding speed of 140 mm/min, which is in disagreement with the results in References [10, 14, 15]. Furthermore, the effect of water cooling on the microstructure and mechanical properties of the FSW 2219Al-T6 joints was investigated [25, 26]. Zhang et al. [25] conducted FSW of 2219Al-T6 under water cooling at rotation rates of 600–1400 rpm and found that the void defects were produced when increasing the rotation rate from 1200 to 1400 rpm. Liu et al. [26] reported that the FSW 2219Al-T6 joints with water cooling at a constant rotation rate of 800 rpm and welding speeds of 50–150 mm/min fractured at either HAZ or NZ; the void defects were produced when increasing the welding speed from 150 to 200 mm/min.

These investigations indicated that void defects easily formed in the FSW 2219Al alloy joints at higher welding speeds or higher rotation rates for both air and cooling conditions [22–26]. However, no detailed explanation about the formation mechanism of void defects was provided in these studies, and the role of welding parameters under a wide range of rotation rates and welding speeds still lacks systematic investigation. Considering the fact that the strength of the FSW precipitation-hardened aluminum alloys could be increased by increasing the welding speed [10, 14, 15], which is highly desirable for industrial production, it is worthwhile to check the feasibility of obtaining sound FSW joints under a higher welding speed for the 2219Al-T6 alloy. Moreover, for practical industrial production, the application of water cooling during FSW is limited because of its special requirement for the equipment. Therefore, FSW investigation under conventional air cooling condition (environment condition) is of greater importance.

In this study, the 2219Al-T6 alloy was subjected to FSW investigation at a wide tool rotation rate range of 400–1600 rpm and a wide welding speed range of 100–800 mm/min. The aim of this study is to (a) explore the possibility to obtain sound FSW 2219Al-T6 joints at a higher welding speed, and (b) elucidate the formation mechanism of defects at a higher welding speed or a higher rotation rate.

Experimental

6.5 mm thick commercial Alclad 2219Al-T6 rolled plates were used in this work as the base metal (BM). The nominal chemical compositions and the tensile properties of the plate are listed in Table 1. The plates, with a length of 400 mm and a width of 90 mm, were machined on both sides to a 5.6 mm thickness to remove the Alclads, and then were butt-welded along the rolling direction with a tool tilt angle of 2.75° using a FSW machine. A tool with a concave shoulder 20 mm in diameter and a conical threaded pin 8 mm in diameter and 5.4 mm in length was used. The FSW parameters used in this study are summarized in Table 2. It should be pointed out that the plunge depth listed in Table 2 is the nominal value displayed on the machine, which is different from the effective plunge depth defined as the depth of the lowest point of the shoulder below the surface of the welded plate. The FSW samples were designated in brief forms. For example, sample 400-100 denotes the sample welded at a rotation rate of 400 rpm and a welding speed of 100 mm/min.

A Vickers microhardness measurement was conducted on the cross-section perpendicular to the welding direction using an automatic testing machine (LECO, LM-247AT)

Table 1 Chemical compositions and mechanical properties of the 2219Al-T6 rolled plate

Chemical composition								Mechanical properties		
Cu	Mg	Mn	Fe	Si	Zn	Ti	Al	YS, MPa	UTS, MPa	EI, Pct
5.8–6.8	0.02	0.2–0.4	0.2	0.2	0.1	0.2–0.1	Bal	342	442	18

Table 2 Welding parameters of FSW 2219Al-T6 joints

Sample	Rotation rate (R), rpm	Welding speed (V), mm/min	Plunge depth, mm	Designation
1	400	100	0.2	400–100
2	800	100	0.1	800–100
3	800	400	0.4	800–400
4	800	800	0.8	800–800
5	1200	100	0.1	1200–100
6	1200	800	0.8	1200–800
7	1600	100	0.05–0.1	1600–100
8	1600	800	0.2–0.8	1600–800

under a load of 500 g for 13 s. The microhardness profiles were obtained along the mid-thickness of the cross-section of the joints. In order to obtain the hardness distribution maps, a total of five test lines were measured throughout the cross section at an interval of 0.5 mm, with a total of 205 indentations. In each line, there were 41 indentations that extended from the weld center to as far as 10 mm on both RS and AS.

All the FSW samples were cross-sectioned perpendicular to the welding direction. Metallographic observation was carried out by optical microscopy (OM, Axiovert 200 MAT). The samples for OM were ground and polished and then etched using Keller's reagent (190 ml water, 2 ml hydrofluoric acid, 3 ml hydrochloric acid and 5 ml nitric acid). The precipitate distributions in the as-welded joints were observed by transmission electron microscopy (TEM TECNAI20). Thin films for TEM observation, which were cut from corresponding locations in the weld using an electrical-discharge machine, were prepared by jet electro polishing using a solution of 70 pct methanol and 30 pct nitric at 243 K (−30 °C) and 19 V. Much care was taken to ensure location-to-location correspondence between the observations and hardness measurements.

In order to obtain the real mechanical properties and fracture locations of the FSW joints, the joint surfaces of tensile specimens were planed with abrasive paper to insure an equal cross-sectional area at various locations of the joints. The configuration and size of the transverse tensile specimens are shown in Fig. 1. Room-temperature tensile tests were carried out at a strain rate of 6×10^{-4} s^{-1} and the tensile properties of each sample

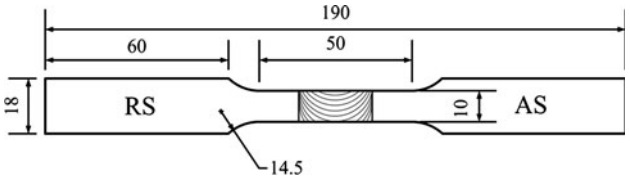

Fig. 1 Configuration and size of tensile specimen (mm)

reported were averages of three test results. The FSW samples for the precipitate observation, hardness, and tension tests were naturally aged at room temperature for more than 10 days.

Results

Joint quality

Figure 2 shows the macrographs of the upper surfaces of the FSW 2219Al-T6 joints under various welding parameters. At a rotation rate of 400 rpm, the joint surface of sample 400-100 was smooth (Fig. 2a). When increasing the rotation rate from 400 to 800 rpm, the joint surface was also smooth under lower welding speeds of 100 and 400 mm/min (Fig. 2b, c) but slight surface delamination was observed on the joint surface at a higher welding speed of 800 mm/min (Fig. 2d). When further increasing the rotation rate from 800 to 1200 rpm, the joint surface not only exhibited a large undulation at a low welding speed of 100 mm/min (Fig. 2e) but also exhibited surface delamination morphology at a high welding speed of 800 mm/min (Fig. 2f). When further increasing the rotation rate from 1200 to 1600 rpm, the obvious tunnel defects were observed at both 100 and 800 mm/min. It should be pointed out that although attempts were made by adjusting the plunge depth in a wide range to avoid void and tunnel defects at a rotation rate of 1600 rpm, sound FSW joints could not be obtained at both lower and higher welding speeds of 100 and 800 mm/min.

Figure 3 shows the macrostructures of the transverse cross sections of the FSW 2219Al-T6 joints. For the tunnel-free FSW joints, no other welding defects were detected in samples 400-100, 800-100, 800-400, 800-800, and 1200-800 (Fig. 3a–d, f), but void defects were observed in sample 1200-100 (Fig. 3e). For sample 1600-100, the tunnel defects were not throughout the whole weld length; the cross section without distinct tunnel defects is presented in Fig. 3g. According to the role of shoulder and pin in the formation of the NZ, the NZ can be subdivided into three sub-zones; i.e., the shoulder-driven zone (SDZ), the pin-driven zone (PDZ), and the swirl zone (SWZ) [28, 29], as shown in Fig. 3e, respectively. It can be seen that a comparatively large PDZ, with regular onion ring structures, and a narrow SDZ were observed in the sound samples 400-100, 800-100, 800-400, 800-800, and 1200-800 (Fig. 3a–d, f). However, a remarkably large SDZ and a shrunken PDZ with irregular onion ring structures were observed in the defective samples 1200-100 and 1600-100 (Fig. 3e, g).

In order to clearly observe the pattern of the defects, the composite macrographs of the white box zones in samples

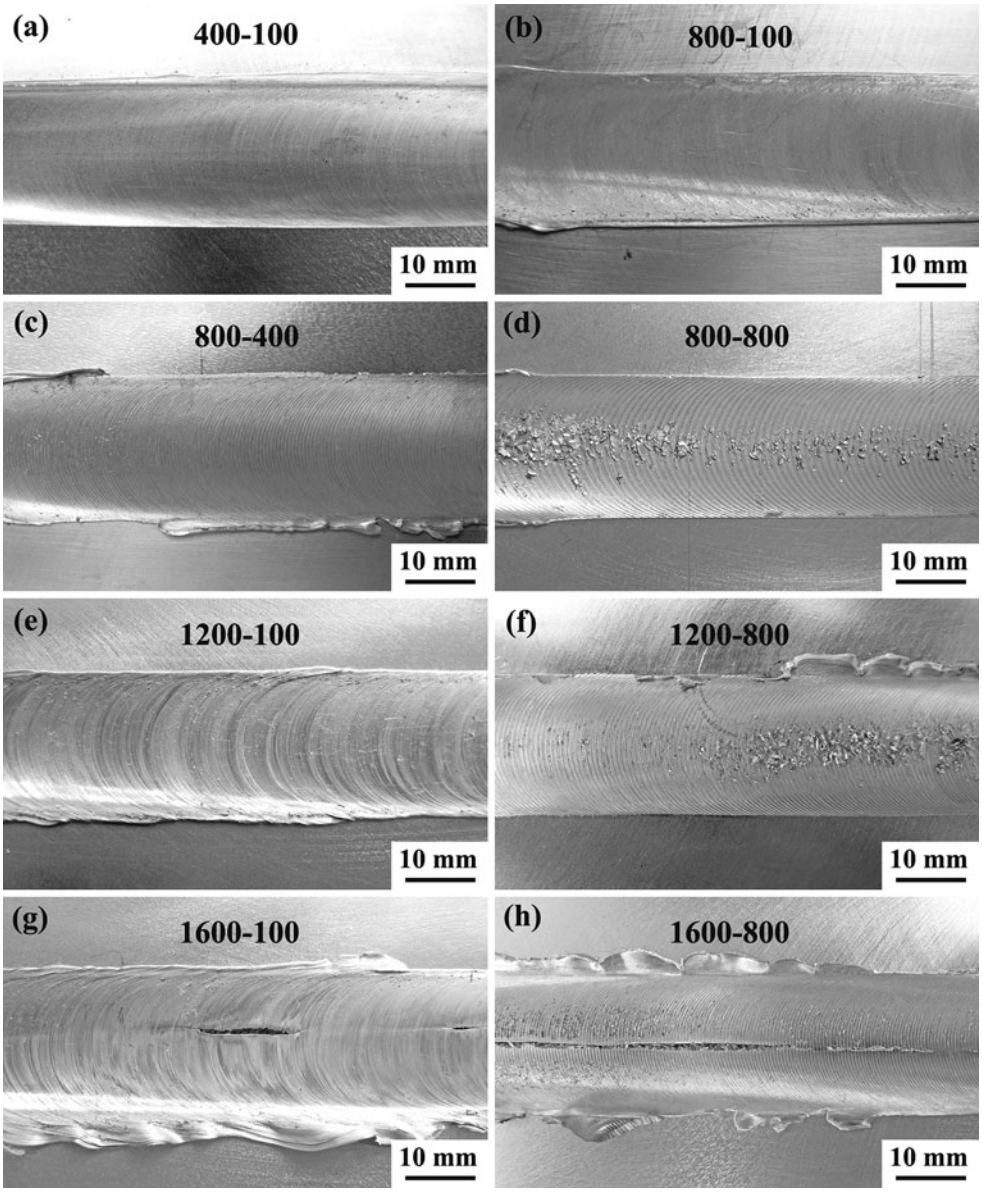

Fig. 2 Surfacial morphologies of FSW 2219Al-T6 joints

1200-100 and 1600-100 (Fig. 3e, g) were constructed as shown in Fig. 4. An extra zone, obviously different from the onion ring structures, existed at the SDZ/PDZ interface of sample 1200-100 on the AS (marked with a black arrow in Fig. 4a). The clear void defects were observed at the extra zone/SDZ and extra zone/PDZ interfaces, respectively. In sample 1600-100, a comparatively large onion ring shaped extra zone was observed at the SDZ/PDZ interface (marked with a black arrow, Fig. 4b).

Microhardness map

Figure 5 shows the microhardness profiles of the FSW 2219Al-T6 joints under the investigated welding parameters. In general, the hardness of the FSW joints was much lower than that of the BM. Two LHZs were observed on the RS and the AS, respectively. The hardness of the LHZ on the RS was lower than that on the AS. Increasing the rotation rate from 400 to 800 rpm at a constant welding speed of 100 mm/min exerted no noticeable influence on the hardness and location of the LHZ, but increased the hardness of the NZ (Fig. 5a). A similar effect was observed when increasing the rotation rate from 800 to 1200 rpm under a higher welding speed of 800 mm/min (Fig. 5b). On the other hand, when increasing the welding speed from 100 to 400 mm/min at a constant rotation rate of 800 rpm, the hardness of the LHZ remarkably increased, resulting in the hardness of the LHZ being close to that of the NZ.

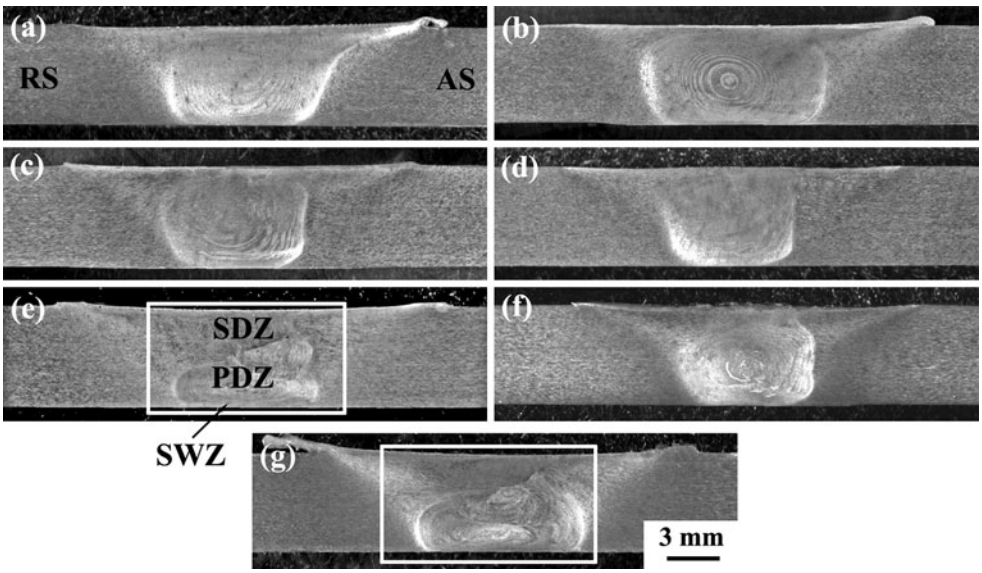

Fig. 3 Cross-sectional macrostructures of FSW 2219Al-T6 joints: (**a**) 400-100, (**b**) 800-100, (**c**) 800-400, (**d**) 800-800, (**e**) 1200-100, (**f**) 1200-800, and (**g**) 1600-100

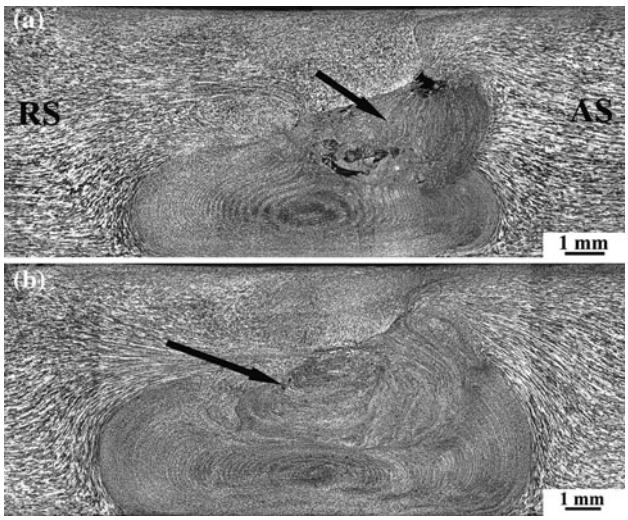

Fig. 4 Magnified images of (**a**) sample 1200-100 and (**b**) sample 1600-100

However, the hardness of the FSW joints was essentially unchanged when further increasing the welding speed from 400 to 800 mm/min at a rotation rate of 800 rpm (Fig. 5c).

It was noted that the above single hardness profile could not predict the fracture path of the FSW 2219Al-T6 joints because of the limited lowest hardness points. In order to accurately predict the fracture behavior of the FSW 2219Al-T6 joints, the microhardness contour maps and the macrographs with the hardness points of samples 800-100 and 800-400 are shown in Figs. 6 and 7, respectively. Two LHZs were obviously observed on both the RS and the AS of sample 800-100 (Fig. 6a). For sample 800-100, it can be determined that the AS LHZ was located at the TMAZ while the RS LHZ was generally located at the NZ/TMAZ interface (marked with dotted lines in Fig. 7a). For sample 800-400, with the increase in the hardness of the LHZ, the hardness of the LHZ was almost identical to the hardness of the NZ (Fig. 6b), and the inconspicuous LHZ was generally located at the HAZ (marked with dotted lines in Fig. 7b). For samples 800-800 and 1200-800, their hardness maps are similar to that of sample 800-400 and are therefore not shown.

Microstructure

Figure 8 shows the OM micrographs of the BM, NZ, TMAZ (AS) and HAZ (AS) of sample 800-400. It can be seen that the elongated grains of the BM resulting from the rolling process were 100–200 μm long and ~10–50 μm wide (Fig. 8a). In the NZ, the microstructure was characterized by the fine and equiaxed recrystallized grains (8–15 μm) arising from the severe plastic deformation and thermal exposure during welding (Fig. 8b). The upward elongated grains were observed in the TMAZ (Fig. 8c), which underwent less plastic deformation and lower heat input. Thus, there was no recrystallization in this zone. Notably coarsened grains were observed in the HAZ (Fig. 8d), at which the plastic deformation was absent and only heat input played a role.

Figure 9a–e shows the bright-field TEM images of the BM, NZ, and LHZs (RS) of samples 800-100 and 800-400. The needle-shaped precipitates Al_2Cu were uniformly distributed in the BM (Fig. 9a). For sample 800-100, only few coarsened Al_2Cu precipitates were observed in the NZ and the diffraction pattern showed that there were no GP

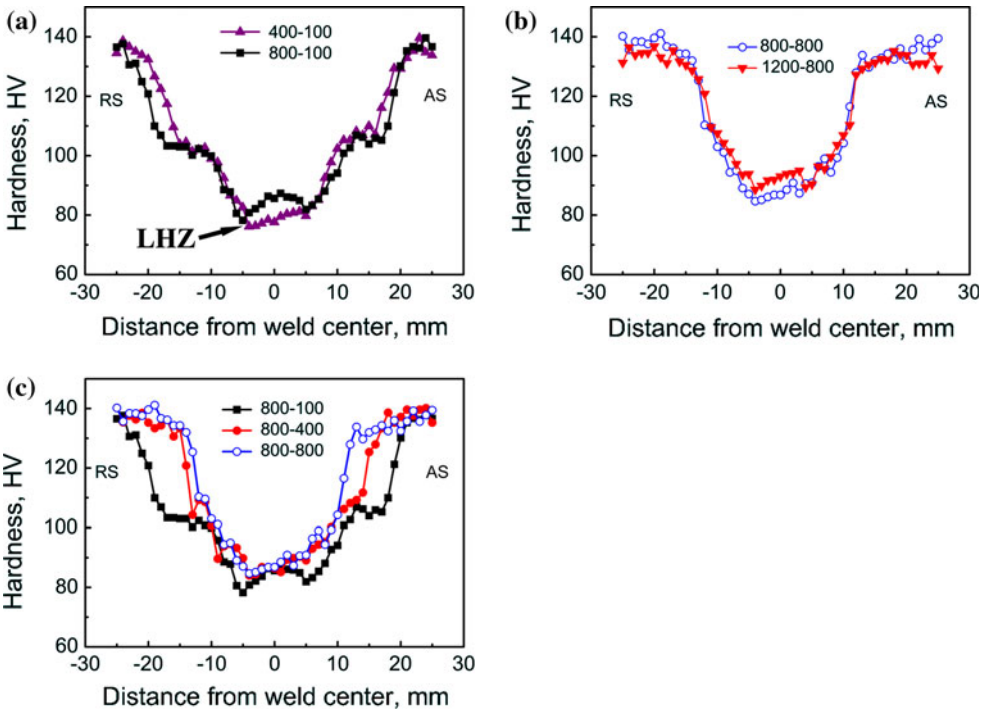

Fig. 5 Microhardness profiles of FSW 2219Al-T6 joints showing effect of rotation rate at (**a**) 100 mm/min, (**b**) 800 mm/min, and (**c**) welding speed at a rotation rate of 800 rpm

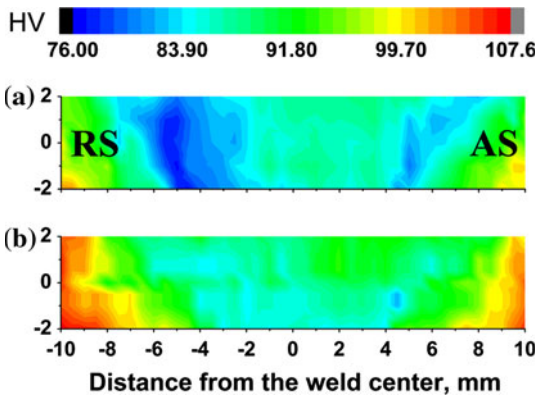

Fig. 6 Microhardness contour maps of (**a**) sample 800-100 and (**b**) sample 800-400

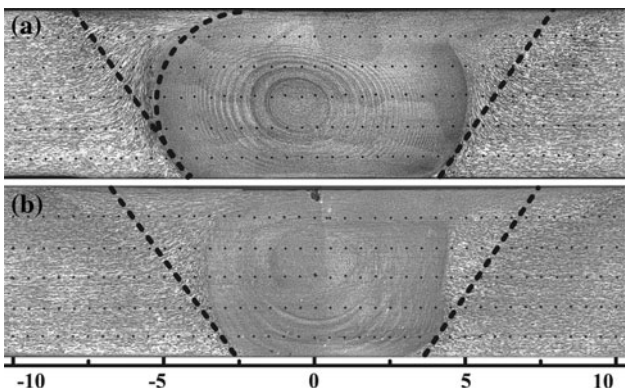

Fig. 7 Location of LHZs (marked by the *black dotted line*) of (**a**) sample 800-100 and (**b**) sample 800-400

zones in the NZ (Fig. 9b). Compared to that in the BM, the density of the Al_2Cu precipitates in the LHZ of sample 800-100 decreased substantially, but their size was much coarser (Fig. 9c). For sample 800-400, the microstructure characteristic in the NZ was nearly identical to that for sample 800-100 (Fig. 9d). Compared with that for sample 800-100, the density of the coarse Al_2Cu precipitates significantly decreased in the LHZ for sample 800-400 (Fig. 9e).

Tensile properties and fracture behavior

The tensile properties of the FSW 2219Al-T6 joints under different welding parameters are shown in Table 3, which reveals two important findings. Firstly, under the constant welding speeds of 100 or 800 mm/min, increasing the rotation rate from 400 to 800 rpm or from 800 to 1200 rpm did not improve the tensile strength of the FSW joints. Secondly, under a constant rotation rate of 800 rpm, the tensile strength sharply increased when increasing the welding speed from 100 to 400 mm/min, but only slightly increased when further increasing the welding speed from 400 to 800 mm/min.

In order to accurately determine the tensile fracture location of the joints, the cross-sections of failed specimens of samples 800-100 and 800-400 were etched, as shown in Fig. 10. It can be seen that sample 800-100 fractured along the LHZ on the RS (Fig. 10a), i.e., the NZ/TMAZ interface on the RS (as shown in Fig. 7a). Sample 800-400 also fractured along the LHZ (HAZ) on the RS (Fig. 10b),

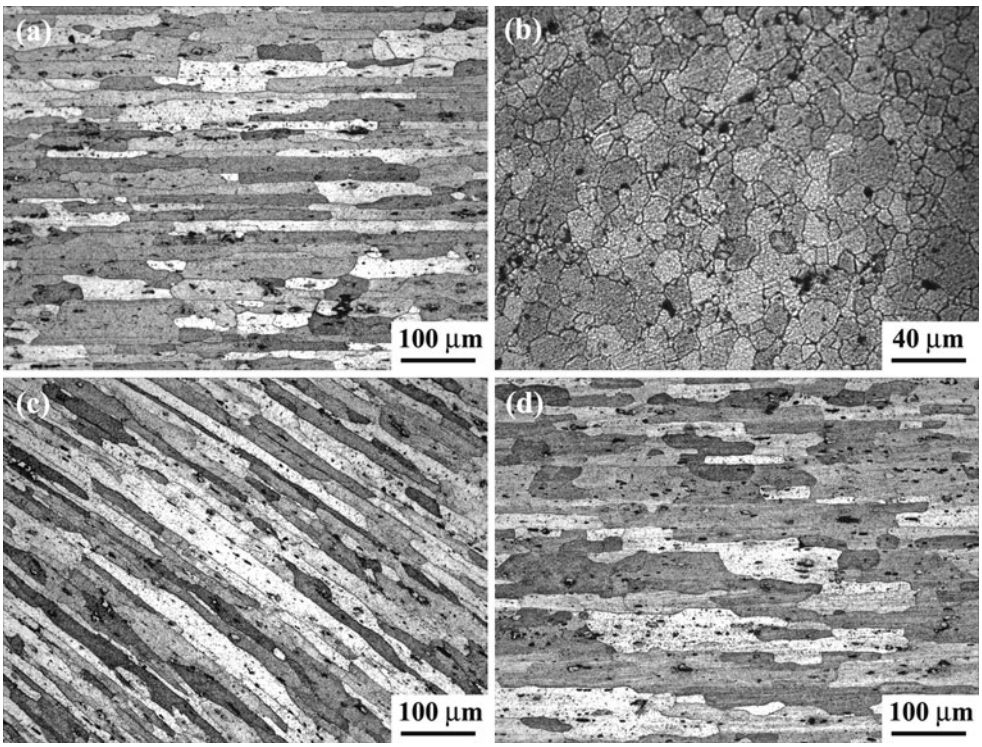

Fig. 8 OM images of (**a**) BM, (**b**) NZ, (**c**) TMAZ (RS), and (**d**) HAZ (RS) of sample 800-400

which was in agreement with the fracture mode reported in References [7, 8]. It should be pointed out that the fracture locations of samples 400-100, 800-800 and 1200-800 were similar to that of sample 800-400.

Figure 11 shows the typical SEM fractographs of samples 800-100 and 800-400. The macroscopic images showed the embossed fracture surface for sample 800-100 but the flat fracture surface for sample 800-400 (Fig. 11a, b). However, the magnified images of positions C and D in samples 800-100 and 800-400 exhibited the similar characteristic of mixed fracture (Fig. 11c, d).

Disscussion

Relationship between welding parameters and joint quality

During FSW, the joint quality was closely related to the material flow. The material flowed around the welding tool, forming a flow field. According to the relationship between material flow characteristic and joint quality during FSW, three material flow states were defined in References [26, 27]; i.e., insufficient material flow, balance material flow and excessive material flow states, respectively. The balance material flow state is an ideal welding state without the occurrence of welding defects. It could be obtained by a reasonable combination of rotation rate, welding speed and plunge depth. The defects were easily produced in the insufficient and excess material flow states, which generally resulted from the high welding speed and rotation rate, respectively [29].

The investigated welding parameters and joint quality for the FSW 2219Al-T6 joints in the previous studies [22–26] and this study are summarized in Table 4. In the previous studies [22–26], the void defects were generally produced at higher rotation rates ($\geq$1300 rpm for air cooling condition or $\geq$1400 rpm for water cooling condition) or high welding speeds ($\geq$300 mm/min for air cooling condition and $\geq$200 mm/min for water cooling condition) for the FSW 2219Al-T6 joints. However, not in complete agreement with the previous results, the results of this study indicated that the quality of the air cooled FSW 2219Al-T6 joint was mainly dependent on the rotation rate rather than the welding speed. The relationship between the welding parameters and the joint quality for the air cooled FSW 2219Al-T6 joints in this study is shown in detail in Fig. 12. Figure 12 showed that the defects (tunnels and voids) mainly existed on the right of the plotted line; i.e., under the higher rotation rates of more than 1200 rpm. This is similar to the rotation rate limit for producing the defect-free FSW 2219Al-T6 joints reported previously [24, 25]. However, the welding speed limit for obtaining the defect-free FSW 2219Al-T6 joints in this study is much higher

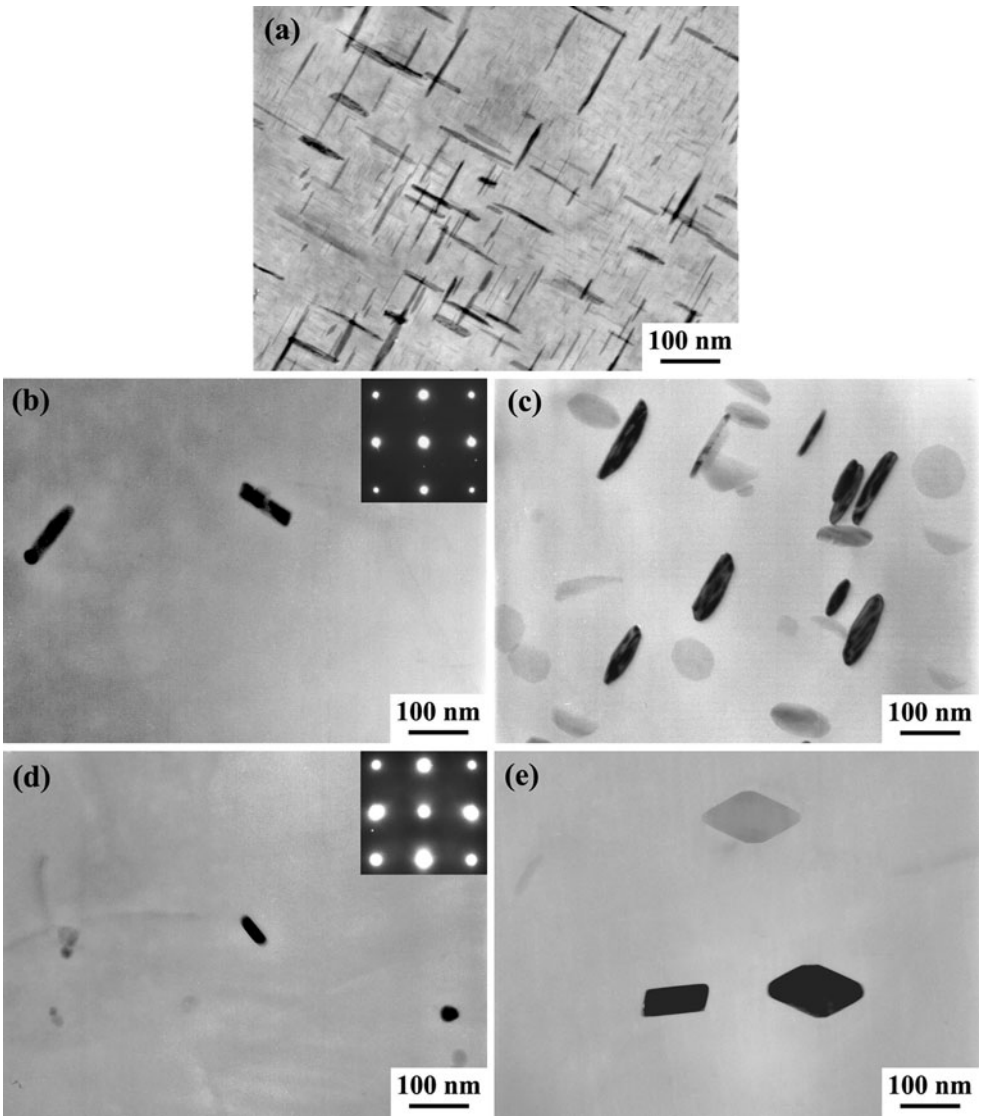

Fig. 9 Bright-field TEM micrographs and associated diffraction patterns in [100] zone axis: (**a**) BM; (**b**) NZ and (**c**) LHZ (RS) of sample 800-100; (**d**) NZ and (**e**) LHZ (RS) of sample 800-400

Table 3 Transverse tensile properties of FSW 2219Al-T6 joints

Sample	El., Pct	UTS, MPa	UTS_{FSW}/UTS_{BM}
400-100	9.0	316 ± 2.0	71.5
800-100	9.0	320 ± 0.7	72.4
800-400	10.0	341 ± 1.0	77.0
800-800	10.0	349 ± 1.0	79.0
1200-800	10.0	346 ± 1.0	78.3

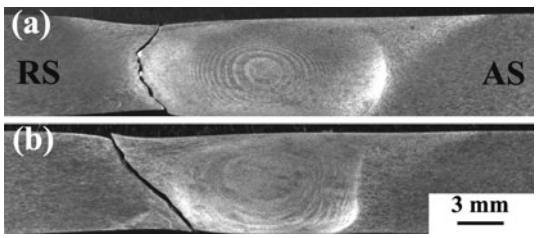

Fig. 10 Fracture locations of (**a**) sample 800-100 and (**b**) sample 800-400

than that reported previously [22, 23]. This difference can be explained as follows.

Besides the rotation rate and welding speed, the plunge depth was also an important welding parameter for FSW [29]. The balance material flow state could be easily obtained under rotation rates of 400 and 800 rpm for a welding speed of 100 mm/min, sound FSW joints were therefore produced (Figs. 2a, b, 3a, b). Increasing the welding speed from 100 to 400 and 800 mm/min would result in the material flow state changing from balance to insufficiency due to inadequate material flow [29].

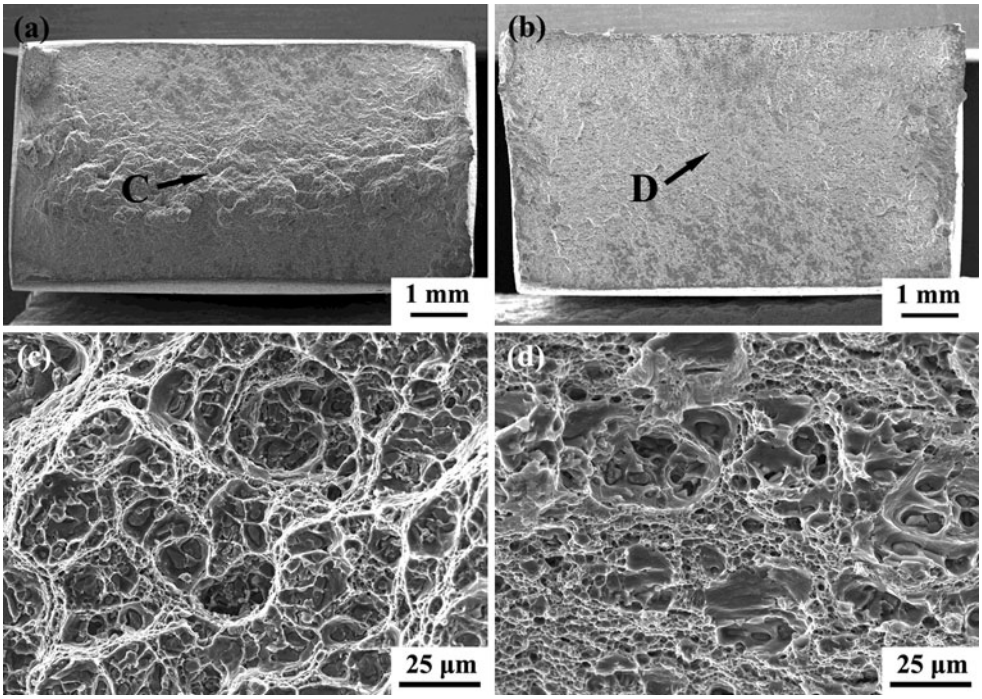

Fig. 11 Fractographs of (**a**) sample 800-100, (**b**) sample 800-400; (**c**) and (**d**) magnified micrographs of marked zones *C* and *D* in Fig. 11a, b, respectively

Table 4 A summary of welding parameters and joint quality of FSW 2219Al-T6 joints

Cooling condition	Investigated welding parameters		Defective sample	References
	Rotation rate	Welding speed		
Air cooling	800	60–300	800-300	[22]
	800	60–300	800-300	[23]
	800–1300	100–140	1300-100	[24]
			1300-140	
	400–1600	100–800	1200-100	This study
			1600-100	
Water cooling	600–1400	100	1400-100	[25]
	800	50–200	800-200	[26]

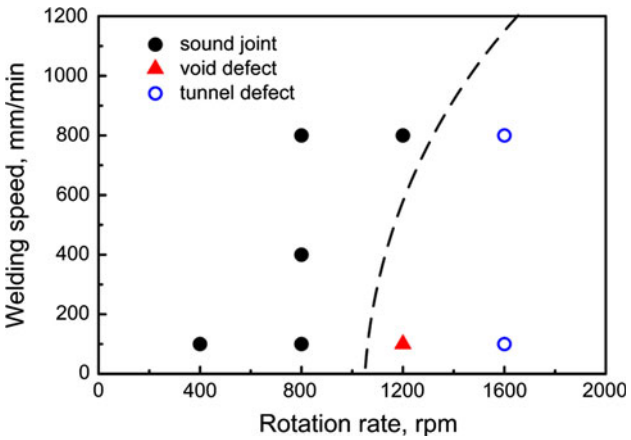

Fig. 12 Welding parameters versus joint quality in FSW 2219Al-T6 joints

However, this could be avoided by properly increasing the plunge depth for the FSW 2219Al-T6 joints. The sound FSW 2219Al-T6 joints were therefore achieved at higher welding speeds of 400 and 800 mm/min (Figs. 2c, d, 3c, d). The void defects in the FSW 2219Al-T6 joints at higher welding speeds reported in References [22–26] may be associated with insufficient plunge depth.

Increasing the rotation rate from 800 to 1200 rpm under a welding speed of 100 mm/min resulted in the material flow state changing from balance to excess. The excessive material flow state drove the excessive material to form an extra zone at the SDZ/PDZ interface (Fig. 4a), disturbing the regular material flow. Thus, void defects were produced in sample 1200-100. The excessive material flow state of sample 1200-100 was not very severe and could be transformed back to the balance material flow state by increasing the welding speed from 100 to 800 mm/min, thereby obtaining a sound joint (Figs. 2f, 3f).

Increasing the rotation rate further from 1200 to 1600 rpm at a welding speed of 100 mm/min made the excessive material flow state more severe in sample 1600-100 than that in sample 1200-100, producing a larger

extra zone at the SDZ/PDZ interface of sample 1600-100 (Fig. 4b). The large extra zone messed up the material flow, resulting in tunnel defects in sample 1600-100 (Fig. 2g). The severe excessive material flow state could not be avoided even by increasing the welding speed from 100 to 800 mm/min and adjusting the plunge depth. The tunnel defects were therefore produced in samples 1600-100 and 1600-800 (Fig. 2g, h).

It should be noted that the material flow is closely related to the plastic deformation ability of the BM. Different aluminum alloys exhibited distinct diversities in the plastic deformation ability. The easily deformed aluminum alloys can generally be welded at comparatively wider welding parameters than the difficultly deformed aluminum alloys. Thus, the relationship between the joint quality and welding parameters may vary with different aluminum alloys.

Relationship between welding parameters and mechanical properties

The fracture location and maximum tensile strength of the FSW 2219-T6 joints in References [22–26], and this study are summarized in Table 5. For the FSW 2219Al-T6 joints, their fracture behavior and mechanical properties were mainly dependent on the microhardness value and distribution of the LHZs, which were closely related to the precipitate distribution of the FSW joints.

Let us focus on the fracture locations of the FSW 2219Al-T6 joints first. Unlike the previous observations that all the LHZs were located in the HAZs of the FSW aluminum alloy joints [22–26], the LHZs may be located at the NZ/TMAZ interface, at the TMAZ or at the HAZ for the FSW 2219Al-T6 joints in this study. Thus, it is worth explaining the controversy about the location of the LHZs before discussing the mechanical properties of the 2219Al-T6 joints.

For the FSW joints of the precipitation-hardened aluminum alloys, the locations of the LHZs are mainly dependent on the precipitate distribution, which is related to the FSW heat input. However, the TMAZ and HAZ were generally identified according to the grain morphology, which was mainly influenced by the geometric shape of the welding tool and the welding parameters. So, there is no direct relationship between LHZs, TMAZ, and HAZ; i.e., the LHZs may be located at the NZ/TMAZ interface, at the TMAZ or at the HAZ for varied welding tools and welding parameters. Especially in this study, the low welding speed of 100 mm/min and a rotation rate of 800 rpm produced a large NZ, leading to the NZ/TMAZ interface overlapping with the LHZs. Thus, the FSW 2219Al-T6 joints reasonably exhibited several different fracture locations in these studies (Table 5).

The mechanical properties of the FSW 2219Al-T6 joints are related mainly to the precipitate distribution of the joints. The 2219Al alloy is a binary Al–Cu alloy and has a certain natural aging tendency. Its precipitation sequence from the supersaturated solid solution (SSSS) is [30]:

$$\text{SSSS} \rightarrow \text{GP zones} \rightarrow \theta\prime \rightarrow \theta\prime\prime \rightarrow \theta.$$

The original Al_2Cu (θ) precipitates in the BM were formed during artificial aging at 190 °C. The precipitates would coarsen at 300–400 °C and dissolve above 505 °C. During FSW, the varied positions of the FSW joints experienced different thermal cycles. The Al_2Cu precipitates therefore evolved in different ways at the varied positions. According to the correlation between the precipitate evolution and the hardness distribution, the FSW 2219Al-T6 joint could be divided into two zones; i.e., dissolution zone and overaging zone (Fig. 13).

The dissolution zone corresponds to the NZ. It experienced severe plastic deformation and high heat input with a peak temperature of about 410–550 °C during FSW [31, 32], resulting in the dissolution of most of the Al_2Cu precipitates as well as the coarsening of the remaining Al_2Cu precipitates (Fig. 9b, d). However, during the subsequent natural aging, the GP zones did not form. A possible reason is that the heating and cooling process of FSW eliminated

Table 5 A summary of fracture location and maximum tensile strength of FSW 2219Al-T6 joints

Cooling condition	Plate thickness, mm	Tensile strength				Fracture location	References
		UTS_{BM}, MPa	Sample	Max UTS_{FSW}, MPa	UTS_{FSW}/UTS_{BM}, %		
Air cooling	5.0	416	800-220	336	81	HAZ	[22, 23]
	6.0	416	1100-140	329	79	No available	[24]
	5.6	442	800-800	349	79	NZ/TMAZ interface, TMAZ or HAZ	This study
Water cooling	7.5	432	800-100	341	79	NZ, NZ/TMAZ interface, or HAZ	[25]
	7.5	432	800-150	347	80	NZ/TMAZ interface or HAZ	[26]

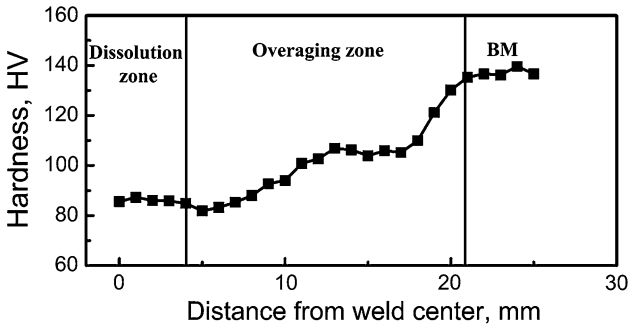

Fig. 13 Schematic diagram showing two sub-zones on transverse cross-section of FSW 2219Al-T6 joints (sample 800-100)

the vacancies, which strongly slowed down the GP zone formation at room temperature after welding. Coupled with the poor natural aging tendency of the 2219Al alloy, the hardness of the NZ was therefore about 85–90 HV. Several investigations showed that, for precipitation-hardened aluminum alloys, the formation of solute clusters, verified by atom probe tomography (APT) technology, could improve the hardness [33–35]. Thus, the difference in the hardness of the NZ of samples 400-100 and 800-100 (Fig. 5a) may result from the solute clusters.

The overaging zone corresponds to the TMAZ and HAZ. This zone experienced thermal cycles with peak temperatures between 200 and 410 °C during FSW [16, 36]. In particular, it was reported that all the LHZs experienced thermal cycles with the same peak temperature of 360–370 °C, and 340 °C for FSW 6061Al-T6 joints [10] and FSW 2024Al-T351 joints [15], respectively. So, it could be conjectured that the FSW 2219Al-T6 joints also experienced similar thermal cycles, resulting in the coarsening of the Al_2Cu precipitates and the formation of the LHZs.

The coarsening degree of the Al_2Cu precipitates was dependent on the duration above the aging temperature of 190 °C; i.e., overaging time, which was related to the welding speed and was independent of the rotation rate [10, 15]. Increasing the welding speed would reduce the overaging time of the Al_2Cu precipitates, and vice versa. Sample 800-100 had a longer overaging time than sample 800-400, indicating a more severe overaging degree in the LHZs of sample 800-100 than that of sample 800-400 (Fig. 9c, e). Thus, both the hardness of the LHZ and the tensile strength of the FSW 2219Al-T6 joints increased when increasing the welding speed from 100 to 400 mm/min (Table 3). It is noted that increasing the welding speed also resulted in a decrease of heat input. Thus, the locations of the LHZs moved inwards (Fig. 5c). This is in agreement with that of FSW joints of 6061Al-T651 [10] and 2024Al-T351 [15]. Probably due to the fast coarsening of the Al_2Cu precipitates, further increasing the welding speed from 400 to 800 mm/min did not improve the hardness of the LHZs (Fig. 5c), but did slightly enhance the tensile strength of sample 800-800 (Table 3). Although, the hardness of the LHZ was close to that of the NZ in samples 800-400 and 800-800 (Fig. 5c), because of the finer grains of the NZ than that of the LHZ, the samples 800-400 and 800-800 fractured along the LHZ.

Under the water cooling condition, some FSW 2219Al-T6 joints were reported to fracture in the NZ [25, 26]. This is probably because the water cooling increased the cooling rate of the LHZs and therefore increased the hardness of the LHZs to the NZ level. Considering that the NZ was the thinnest zone of the FSW joint due to a $\sim 3°$ tilt angle of the welding tool and the plunge depth, it was reasonable that the water cooled FSW 2219Al-T6 joints fractured in the NZ.

The results of this study demonstrate the close relationship between the welding parameters, joint quality, and mechanical properties for the FSW 2219Al-T6 joints. Firstly, in order to obtain a sound FSW joint, the rotation rate should be less than 1200 rpm. However, there are a wide range of welding speeds between 100 and 800 mm/min available for producing defect-free joints, with optimized plunge depth. Secondly, the effect of water cooling on the tensile strength of the FSW 2219Al-T6 joints was not clear due to lack of direct contrast with the air cooled FSW joints in References [25, 26]. However, from Table 5, it seems that the water cooling does not produce a positive effect on the tensile strength of the FSW 2219Al-T6 joints, and the maximum tensile strength of the FSW joints was generally not larger than 80% of that of the BM. The effect of the water cooling on the mechanical properties of the FSW 2219Al-T6 joints needs an additional study.

Conclusions

1. There existed an optimal range of FSW parameters for the 2219Al-T6 alloy. Sound FSW joints could be obtained under lower rotation rates of 400–800 rpm for welding speeds of 100–800 mm/min. High rotation rates of 1200–1600 rpm easily resulted in tunnel and void defects.
2. The FSW thermal cycle resulted in the LHZs on both RS and AS due to the dissolution and coarsening of Al_2Cu precipitates. The hardness of the LHZs increased as the welding speed increased from 100 to 400 mm/min, but was essentially unchanged when further increasing the welding speed from 400 to 800 mm/min at a rotation rate of 800 rpm. However, the hardness of the LHZs was independent of the rotation rates ranging from 400 to 1200 rpm.

3. The LHZs of the FSW 2219Al-T6 joints may be located at the NZ/TMAZ interface, at the TMAZ, or at the HAZ under different welding parameters.
4. The FSW 2219Al-T6 joints fractured along the LHZs on the RS. The tensile strength of the joints increased as the welding speed increased from 100 to 800 mm/min and was independent of the rotation rates ranging from 400 to 1200 rpm. The maximum tensile strength of the FSW 2219Al-T6 joints was 79% of that of the BM.

Acknowledgements The authors gratefully acknowledge the support of the Hundred Talents Project of Chinese Academy of Sciences and the National Outstanding Young Scientist Foundation with Grant No. 50525103.

References

1. Kamp N, Gao N, Starink MJ, Sinclair I (2007) Int J Fatigue 29:869
2. Majimel J, Casanove MJ, Molénat G (2004) Mater Sci Eng A 380:110
3. Wang HX, Wei YH, Yang CL (2007) Comput Mater Sci 38:571
4. Rao SRK, Reddy GM, Rao KS, Kamaraja M, Rao KP (2005) Mater Charact 55:345
5. Thomas WM, Nicholas ED, Needham JC, Murch MG, Templesmith P, Dawes CJ (1991) GB Patent Application No. 9125978.8, 6 Dec 1991
6. Mishra RS, Ma ZY (2005) Mater Sci Eng R 50:1
7. Schneider JA, Nunes AC Jr, Chen PS, Steele G (2005) J Mater Sci 40:4341. doi:10.1007/s10853-005-2808-8
8. Krishnan KN (2002) J Mater Sci 37:473. doi:10.1023/A:1013701104029
9. Ren SR, Ma ZY, Chen LQ (2007) Scripta Mater 56:69
10. Liu FC, Ma ZY (2008) Metall Mater Trans A 39:2378
11. Fuller CB, Mahoney MW, Calabrese M, Micona L (2010) Mater Sci Eng A 527:2233
12. Brown R, Tang W, Reynolds AP (2009) Mater Sci Eng A 513–514:115
13. Mahoney MW, Rhodes CG, Flintoff JG, Spurling RA, Bingel WH (1998) Metal Mater Trans A 29:1955
14. Zhao YH, Lin SB, Wu L, Qu FX (2005) Trans Nonferrous Met Soc China 15:1248
15. Zhang Z, Xiao BL, Ma ZY Acta Mater (under review)
16. Lee WB, Yeon YM, Jung SB (2004) Mater Trans 45:1700
17. Lim S, Kim S, Lee C, Lee CG, Kim S (2004) Metall Mater Trans A 35:2829
18. Liu HJ, Fujii H, Nogi K (2005) J Mater Sci 40:3297. doi:10.1007/s10853-005-2705-1
19. Zhang XX, Xiao BL, Ma ZY (2011) Metall Mater Trans A 42:3218
20. Zhang XX, Xiao BL, Ma ZY (2011) Metall Mater Trans A 42:3229
21. Zhang Z, Xiao BL, Ma ZY Metall Master Trans A (under review)
22. Chen YC, Liu HJ, Feng JC (2006) Mater Sci Eng A 21:420
23. Liu HJ, Chen YC, Feng JC (2006) Mater Sci Technol 22:237
24. Xu WF, Liu JH, Luan GH, Dong CL (2009) Mater Des 30:3460
25. Zhang HJ, Liu HJ, Yu L (2011) Mater Des 32:4402
26. Liu HJ, Zhang HJ, Yu L (2011) Mater Des 32:1548
27. Kumar K, Kailas SV (2008) Mater Sci Eng A 485:367
28. Arbegast WJ (2008) Scripta Mater 58:372
29. Zhang Z, Xiao BL, Wang D, Ma ZY (2011) Metall Mater Trans A 42:1717
30. Lorimer GW (1978) Precipitation processes in solids. TMS-AIME, Warrendale, p 87
31. Colegrove PA, Shercliff HR (2003) Sci Technol Weld Join 8:360
32. Sato YS, Urata M, Kokawa H (2002) Metall Mater Trans A 33:625
33. Marceau RKW, Sha G, Ferragut R, Dupasquier A, Ringer SP (2010) Acta Mater 58:4923
34. Pogatscher S, Antrekowitsch H, Leitner H, Ebner T, Uggowitzer PJ (2011) Acta Mater 59:3352
35. Marlaud T, Deschamps A, Bley F, Lefebvre W, Baroux B (2010) Acta Mater 58:4814
36. Xu WF, Liu JH, Luan GH, Dong CL (2009) Mater Des 30:1886